In-line Fabry-Perot refractive index sensor based on microcavity

Feng Xu (徐 峰), Lu Lu (卢 璐), Weiwei Lü (吕卫卫), and Benli Yu (俞本立)*

School of Physics and Materials Science, Anhui University, Hefei 230601, China

**Corresponding author: benliyu@ahu.edu.cn*

Received March 25, 2013; accepted May 13, 2013; posted online August 2, 2013

An in-line Fabry-Perot (FP) refractive index (RI) sensor based on an intrinsic FP cavity and fabricated by the etching and fusion splicing method is proposed. The experimental results demonstrate that the sensor possesses a high resolution of 1508 nm/RIU for the measurement of acetylene gas RI. The temperature-response measurement shows that the sensor is insensitive to room temperature variations. The FP RI sensor is suitable for applications in biosensing and environmental monitoring because of its high sensitivity and structural simplicity, thereby making it suitable for low-cost mass production.

OCIS codes: 280.4788, 280.1415.

doi: 10.3788/COL201311.082802.

Fiber-optic refractive index (RI) sensors have attracted considerable interest in recent years because of their outstanding advantages over conventional sensors, including their high sensitivity, compact size, immunity to electromagnetic interference, and remote sensing capability. These characteristics make fiber-optic RI sensors suitable for applications such as biomedical research, health care, and environmental monitoring. Many different types of fiber-optic RI sensors have been proposed based on tapered fibers, fiber grating, and surface plasma resonance[1−9]. The in-line Fabry-Perot interferometer (FPI) sensor is one of the most important categories of fiber-optic RI sensors[10−12]. A distinct advantage of an FPI sensor over other types of fiber-optic RI sensors is that it can easily isolate RI measurements from the effects of temperature variations. Therefore, this sensor can provide absolute RI information. In general, an in-line FPI sensor consists of an FP cavity and a microchannel, which is typically formed directly on a fiber end face. The wavelength-dependent interference fringe pattern of the FPI sensor depends on the RI of the material filled in the cavity. Therefore, RI can be determined by measuring the interference fringe patterns. To allow liquid or gas to flow into the cavity during measurements, a microchannel is generally used to guide the fluids into the cavity. This microchannel is a key feature of an in-line FPI and has to be considered in the fabrication process. Although laser micromachining can be used to fabricate such a micro-channel[13], it is not a method suitable for mass production. Furthermore, the microchannel located near the fiber core decreases the intensity of the optical signal reflected from the FP cavity. As a result, the accuracy of the FPI sensor deteriorates because of the decreased interference fringe contrast.

In this letter, we propose and experimentally demonstrate a novel hybrid, in-line FP RI sensor based on an intrinsic FP cavity. This in-line FP RI sensor consists of an etched graded-index fiber (GIF) and a short piece of polarization maintenance photonic crystal fiber (PM-PCF). The fabrication process consists of two steps, namely, fiber etching and fusion splicing. We investigate the performance of the proposed FPI sensor in RI measurements. The experimental results indicate that the sensor is highly sensitive to the RI of the material under study. In addition, it is insensitive to ambient temperature variations.

The scheme of the proposed in-line FP RI sensor is illustrated in Fig. 1. The sensor was formed by splicing a short piece of GIF (core diameter, 62.5 μm) to a conventional single-mode fiber (SMF, SMF-28, Corning, USA). The cavity at the GIF tip was fabricated by etching. A short section of the PM-PCF was then spliced on the right side of the GIF and carefully cleaved to form an FP cavity. The PM-PCF air holes act as microchannels between the external air and the cavity and thus serve as an entrance to the cavity. Light propagates through the cavity and is then reflected by the two sides of the air gap. The right side of the PCF slice was cleaved at an angle of $\sim$8° to reduce the reflection of the fiber end. This process ensures that the peaks of the interference fringe pattern are sharp and easily distinguishable because of the two-beam interference. The technique also improves the detection accuracy.

The specific fabrication process of the FP sensor consists of two steps (Fig. 2). The first step involves splicing an SMF to a short section of the GIF. Afterward, the GIF end was cleaved and chemically etched by immersing in 40% HF for 2.5 min. The etching rate of the GIF core, which is composed of Ge silica, is higher than that of the cladding. A concavity with a depth of approximately 40 μm was therefore created, whereas the outer diameter of the GIF cladding remained unchanged at the end of the etching process. This process ensures that the subsequent fusion splicing step is straightforward because

Fig. 1. (Color online) Scheme of the in-line FP RI sensor. SM: single-mode fiber; GIF: graded-index fiber.

the material property of the fiber cladding at the splicing point is not affected by etching. To form the intrinsic FP cavity, we spliced the etched GIF to a short section of the PM-PCF instead of using a laser micromachining method. The PM-PCF has a cladding that consists of five-ring air holes arranged in a hexagonal pattern. The diameters of the air holes and of the entire solid region are 2.5 and 5 μm, respectively. Two big air holes with 5-μm diameters replaced the two small air holes of the first ring to maintain the polarization. The small air holes of the PM-PCF completely collapsed after the splicing process. However, the two big air holes remained and served as two microchannels between the FP cavity and the external air. A fusion splicer (FSM-60s Fujikura, Japan) was used to fabricate the sensor, and the splicing parameters were carefully selected to preserve the structural integrity of the PCF and form the microchannel. We used a prefuse time of 50 ms. The discharge electric intensity was fixed at a "standard-39 bit," and the "overlap" for fusion splicing was set at 10 μm. The PM-PCF was cleaved after the FP cavity was formed. We cleaved the PM-PCF at an angle of ~8° to eliminate the reflection of the fiber face. Therefore, the cavity produced a two-beam interference. Compared with the laser micromachine fabrication technique, the fusion splicing method provides a simpler and low-cost fabrication process. Furthermore, the two off-center channels minimize the reduction in face reflectivity compared with the structure with the channel in the center. The two off-center air

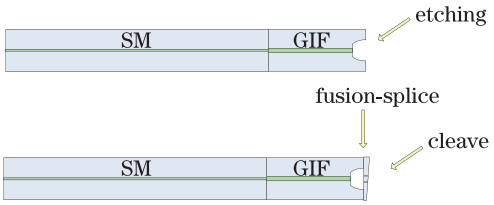

Fig. 2. (Color online) Fabrication process of the proposed sensor: (a) GIF tip etching and (b) GIF spliced to a short section of the PM-PCF.

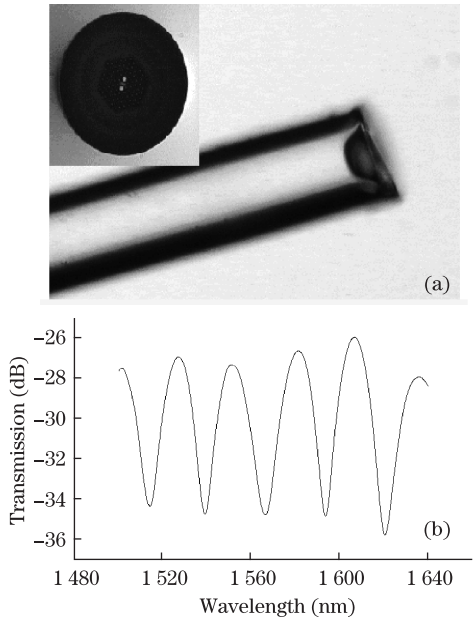

Fig. 3. (a) Image and (b) interference spectrum of the FP interferometer sensor.

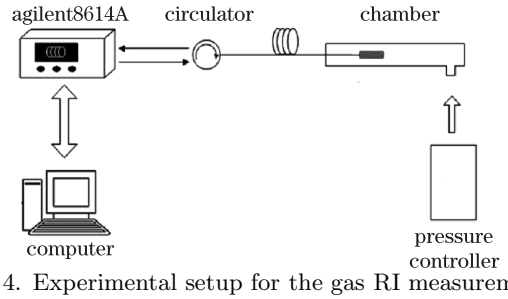

Fig. 4. Experimental setup for the gas RI measurement.

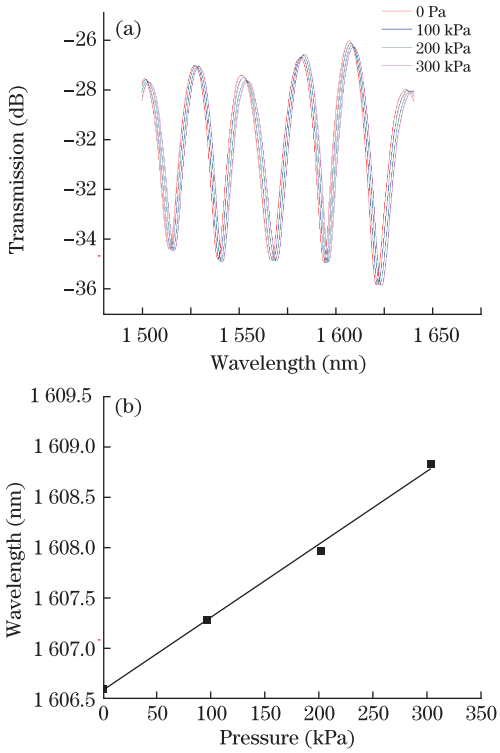

Fig. 5. (Color online) (a) Interference spectra of the sensor in air and (b) wavelength shift of the proposed sensor at different pressures.

holes in the proposed structure help improve the interference fringe contrast while conveniently guiding the liquid or gas in and out the cavity.

The in-line FP RI sensor was fabricated (Fig. 3(a)) by using the aforementioned method. The inset in Fig. 3(a) shows the cross-section of the PM-PCF used in this structure. The interference spectrum of this sensor in air is shown in Fig. 3(b). The recorded spectrum indicates a fringe contrast of ~10 dB, which is higher than the typical fringe contrast of ~5 dB in a previously reported FPI-based fiber sensor[14]. This increased fringe contrast is an important advantage of the proposed sensor and may be used to improve the measurement accuracy significantly in practical applications.

As mentioned above, two adjacent peaks in the interference fringe have a phase difference of 2π because of FP interference. Therefore, the optical path length of the cavity can be calculated by

$$nL = \frac{\lambda_1 \lambda_2}{2(\lambda_1 - \lambda_2)}, \tag{1}$$

where λ_1 and λ_2 are the wavelengths of the two adjacent peaks (Fig. 3 (b)), L is the cavity length, and n is the

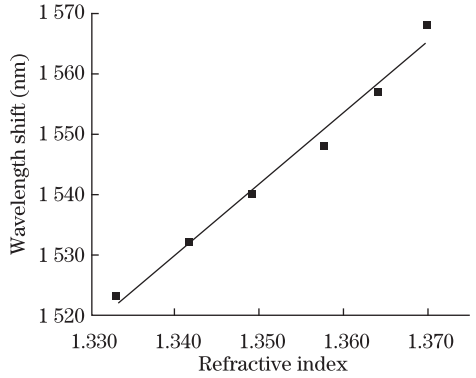

Fig. 6. Wavelength shift of the interference spectrum of the sensor in different sugar solution concentrations.

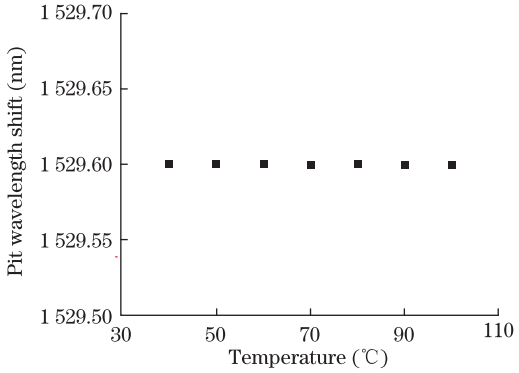

Fig. 7. Temperature characteristic of the proposed sensor.

RI of the medium filled in the cavity. Hence, the RI of an unknown medium can be obtained from Eq. (1) if the interference fringe pattern is measured.

We conducted RI measurements to evaluate the performance of the proposed sensor in RI sensing. The experimental setup is shown in Fig. 4. The sensor was placed inside a pressure chamber to regulate the pressure applied on the sensor from 0 to 300 kPa. The testing gas was pure acetylene. The interference fringe patterns corresponding to different pressure levels are shown in Fig. 5(a). These results were obtained with a wavelength-swept laser interrogator (8164A, Agilent, USA) at a resolution of 0.1 pm. Figure 5(b) shows that the peaks of the interference fringe pattern shift to long wavelengths as the pressure increased. Given that the RI of the gases is a function of density, which in turn depends on the pressure, the gas RI can be calculated at different pressures according to the Gladstone-Dale model[15]. The sensitivity of the proposed sensor is approximately 1 508 nm/RIU. The minimum detectable change in RI is 6.6×10^{-8} at a resolution of 0.1 pm. The measurement results also show a reasonably good linearity, with a correlation coefficient of 0.9963. The sensitivity of the sensor is mainly attributed to its high fringe contrast.

In addition to the index measurement of gas, we also applied the RI sensor in a liquid sensing experiment. In this experiment, the sensor head was dipped in different concentrations of a sugar solution. Figure 6 shows that the wavelength of the interference spectrum shifts with the change in the RI. The RI resolution is ∼1 180 490 nm/RI, with a linearity of ∼99.068%. The minimum detectable change in RI is 8.4×10^{-8} at a resolution of 0.1 pm. The sensitivity of the sensor is lower than that of the gas measurement, which results from the difference between the RI of the sugar solution (ranging from 1.3 to 1.7) and that of acetylene.

The temperature dependence of the proposed sensor was also investigated (Fig. 6). The sensor head was placed in a temperature-controlled chamber to determine the effects of different temperatures (from 40 to 100 °C). Figure 7 shows the measured wavelength of the FP reflection peak at approximately 1 529.6 nm. No measurable peak wavelength shift over the 40 to 100 °C temperature range is observed. The temperature response of the sensor indicates that it can operate at room temperature without the need for additional temperature control and compensation. This temperature independence results from the low thermal expansion coefficient of pure silica (0.55×10^{-6} /°C) as well as from the open cavity in the sensor configuration.

In conclusion, we experimentally demonstrate a high-sensitivity in-line FP RI sensor based on a fiber FP cavity. The cavity is fabricated by chemical etching, fusion splicing, and cleaving. PCF air-holes are used as microchannels to guide fluids in and out of the cavity. The fabrication of this high-quality FP RI sensor is simple and potentially low-cost. The sensor possesses a high resolution of 1 508 nm/RIU for acetylene gas and 1180 nm/RIU for a sugar solution while maintaining its temperature insensitivity. The experimental results prove that the FP RI sensor is suitable for applications in biosensing and environmental monitoring because of its high-sensitivity and structural simplicity, which allow for low-cost mass production.

This work was supported by the National Natural Science Foundation of China (No. 61108076), the Open Foundation of National Laboratory for Infrared Physics, Chinese Academy of Science (No. 201007), the Key Research Project of the Anhui Education Department (No. KJ2011A009), and the "211" Project of Anhui University. Special thanks are given to Prof. Rongqing Hui of the Department of Electrical Engineering and Computer Science, University of Kansas for the discussions and advices.

References

1. X. Wu, J. Zhang, J. Chen, C. Zhao, and Q. Gong, Opt. Lett. **34,** 392 (2009).
2. Y. L. Lo, C. H. Chuang, and Z. W. Lin, Opt. Lett. **36,** 2489 (2011).
3. F. Xu, C. Li, D. Ren, L. Lu, and W. Lu, Chin. Opt. Lett. **10,** 070603 (2012).
4. D. K. C. Wu, B. T. Kuhlmey, and B. J. Eggleton, Opt. Lett. **34,** 322 (2009).
5. B. Wang, T. Siahaan, M. A. Dündar, R. Nötzel, M. J. van der Hoek, S. He, and R. W. van der Heijden, Opt. Lett. **37,** 833 (2012).
6. K. Mileńko, D. J. J. Hu, P. P. Shum, T. Zhang, J. L. Lim, Y. Wang, T. R. Woliński, H. Wei, and W. Tong, Opt. Lett. **37,** 1373 (2012).
7. Y. Cao, Y. Yang, X. Yang, and Z. Tong, Chin. Opt. Lett. **10,** 030605 (2012).
8. N. Lin, L. Jiang, S. Wang, L. Yuan, and Q. Chen, Chin.

Opt. Lett. **10,** 052802 (2012).

9. G. Xin, K. Peng, Z. Gu, J. Zhao, R. Fan, L. Liu, and X. Xu, Chin. Opt. Lett. **11,** 020601 (2013).
10. Q. Liu and Q. Wang, Chin. Opt. Lett. **10,** 090601 (2012).
11. Y. Ma, X. Qiao, T. Guo, R. Wang, J. Zhang, Y. Weng, Q. Rong, M. Hu, and Z. Feng, Chin. Opt. Lett. **10,** 050603 (2012).
12. E. Cibula and D. Donlagic, Opt. Express **15,** 8719 (2007).
13. Z. Ran, Y. Rao, J. Zhang, Z. Liu, and B. Xu, J. Lightwave Technol. **27,** 5426 (2009).
14. L. Coelho, P. A. R. Tafulo, P. A. S. Jorge, J. L. Santos, D. Viegas, K. Schuster, J. Kobelke, and O. Frazão, Opt. Lett. **37,** 3063 (2012).
15. J. T. Robinson, L. Chen, and M. Lipson, Opt. Express **16,** 4296 (2008).